9

Studies on the Interaction Between an Acoustic Wave and Levitated Microparticles

Ovidiu S. Stoican
National Institute for Laser, Plasma and Radiation Physics - Magurele
Romania

1. Introduction

The electrode systems generating a quadrupole electric field, having both static and variable components, under certain conditions, allow to maintain the charged particles in a well defined region of space without physical solid contact with the wall of a container. This process is sometime called *levitation*. Usually, these kinds of devices are known as *quadrupole traps*. The operation of a quadrupole trap is based on the *strong focusing* principle (Wuerker et al., 1959) used most of all in optics and accelerator physics. Due to the impressive results as high-resolution spectroscopy, frequency standards or quantum computing, the research has been directed mainly to the ion trapping. Wolfgang Paul, who is credited with the invention of the quadrupole ion trap, shared the Nobel Prize in Physics in 1989 for this work. Although less known, an important amount of scientific work has been deployed to develop similar devices able to store micrometer sized particles, so-called *microparticles*. Depending on the size and nature of the charged microparticles to be stored, various types of quadrupole traps have been successfully used as a part of the experimental setups aimed to study different physical characteristics of the dust particles (Schlemmer et al., 2001), aerosols (Carleton et al., 1997; Davis, 1997), liquid droplets (Jakubczyk et al., 2001; Shaw et al., 2000) or microorganisms (Peng et al., 2004). In this paper the main outlines of a study regarding the effect of a low frequency acoustic wave on a microparticles cloud which levitates at normal temperature and atmospheric pressure within a quadrupole trap are presented. The acoustic wave generates a supplementary oscillating force field superimposed to the electric field produced by the quadrupole trap electrodes. The aim of this experimental approach is evaluating the possibility to manipulate the stored microparticles by using an acoustic wave. That means both controlling their position in space and performing a further selection of the stored microparticles. It is known that, as a function of the trap working parameters, only microparticles whose charge-to-mass ratio Q/M lies in a certain range can be stored. Such a selection is not always enough for some applications. In the case of a conventional quadrupole trap where electrical forces act, particle dynamic depends on its charge-to-mass ratio Q/M. Because the action of the acoustic wave is purely mechanical, it is possible decoupling the mass M and the electric charge Q, respectively, from equation of motion. An acoustic wave can be considered as a force field which acts remotely on the stored microparticles. There are two important parameters which characterize an acoustic wave, namely wave intensity and frequency. Both of them can be varied over a wide range so that the acoustic wave mechanical effect can be settled very precisely. The experiments have been focused on the acoustic

frequency range around the frequency of the ac voltage applied to the trap electrodes, where resonance effects are expected. Comparisons between experimental results and numerical simulations are included.

2. Linear electrodynamic trap

To store the micrometer sized particles (microparticules), in air, at normal temperature and pressure, the electrodes system shown in Fig.1 has been used. The six electrodes consist of four identical rods (E1, E2, E3, E4), equidistantly spaced, and two end-cap disks (E5, E6). The rod electrodes E2 and E3 are connected to a high ac sinusoidal voltage $V_{ac} = V_0 cos 2\pi f_0 t$. The electrode E4 is connected to a dc voltage U_x while the electrode E1 is connected to the ground. The end-caps electrodes E5, E6 are connected to a dc voltage U_z. Such an electrodes arrangement is known as a *linear electrodynamic trap*. A linear electrodynamic trap is characterized by a simple mechanical layout, confines a large number of microparticles and offers good optical access. For an ideal linear electrodynamic trap, near the longitudinal axis $x, y \ll R$, assuming $L_z \gg R$ and neglecting geometric losses, the electric potential may be expressed approximately as a quadrupolar form (Major et al., 2005; Pedregosa et al., 2010):

$$\phi(x, y, t) = \frac{(x^2 - y^2)}{2R^2}(U_0 + V_0 cos\Omega t) \tag{1}$$

where R is the inner radius of the trap and $\Omega = 2\pi f_0$. The voltage Uz assures the axial stability of the stored particles while the electric field due to the voltage U_x balances the gravity force. In the particular case of the linear electrodynamic trap used in this work, the diameter of the rods and distance between two opposite rods are both 10 mm, therefore R=5 mm. The distance L_z between the end-cap disk electrodes can be varied between 30 mm and 70 mm. During the experiments, the distance L_z has been kept at 35 mm. The dc voltages U_z and U_x can be varied in the range 0-1000V, while the ac voltage V_{ac} is on the order of 1-4kV_{rms} at a frequency from 40 to 100 Hz. The usual values for the voltages applied to trap electrodes are summarized in Table 1. Microparticles cloud is confined in a narrow region along the longitudinal trap

Voltage	Electrode	Range	Frequency
$V_{ac} = V_0 cos 2\pi f_0 t$	E2 and E3	V_0=1-4kV	40-100Hz
U_x	E4	0-1000V	dc
U_z	E5 and E6	0-1000V	dc

Table 1. Summary of the electric voltages applied to the linear trap electrodes.The electrode E1 is connected to ground.

axis (see Fig.2). To avoid the perturbations produced by the air streams the whole trap is placed inside a transparent plastic box. The charged microparticles are stored inside the trap for hours in a quasi interaction free environment. More details on the linear electrodynamic traps mechanical layout can be found in (Gheorghe et al., 1998; Stoican et al., 2001). The motion of a charged particle in a quadrupole electric field is very well known e.g. (Major et al., 2005; March, 1997) and an extensive review are beyond the scope of this paper. Here will be summarized only the basic equations necessary to perform an appropriate numerical analysis of the effect of an acoustic field on the stored microparticles. Taking into account the expression (1) of the electric potential and the presence of a supplementary force due to the

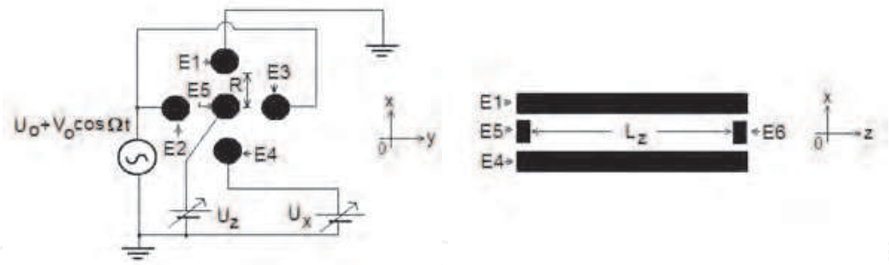

(a) View of the section xy (b) View of the section xz

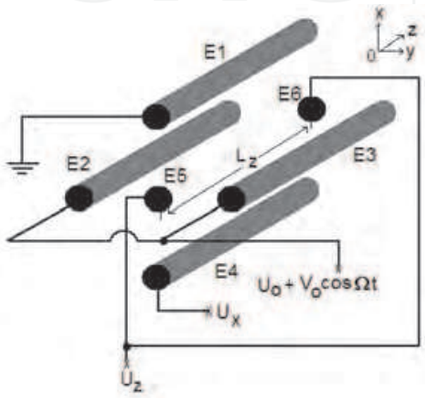

(c) 3D view

Fig. 1. Schematic drawing and electrodes wiring of a linear electrodynamic trap. The drawings are not to scale.

acoustic field, equations of motion in the (x,y) plane for a charged particle of mass M and charge Q, located near the linear trap axis, are:

$$M\frac{d^2x}{dt^2} = -\frac{Qx}{R^2}(U_0 + V_0 cos\Omega t) - k\frac{dx}{dt} + F_{Ax}(t) \tag{2}$$

and

$$M\frac{d^2y}{dt^2} = \frac{Qy}{R^2}(U_0 + V_0 cos\Omega t) - k\frac{dy}{dt} + F_{Ay}(t) \tag{3}$$

The terms $-k\frac{dx}{dt}$ and $-k\frac{dy}{dt}$, describe the drag force exerted on an object moving in a fluid. Assuming that the particles are spherical, according to *Stokes's law*:

$$k = 6\pi\eta(d/2) \tag{4}$$

where d is the diameter of the charged particle while $\eta \approx 1.8\text{x}10^{-5}\text{kgm}^{-1}\text{s}^{-1}$ is the air viscosity at normal pressure and temperature. The time-depended terms $F_{Ax}(t)$ and $F_{Ay}(t)$, stand for the force exerted by the acoustic wave on the stored particle. The Ox is the vertical axis. The microparticles weight has been neglected. Making change of variable $\xi = \Omega t/2$ the equations (2) and (3) can be rewritten as:

$$\frac{d^2x}{d\xi^2} + \delta\frac{dx}{d\xi} + (a_x + 2q_x cos2\xi)x - s_{Ax} = 0 \tag{5}$$

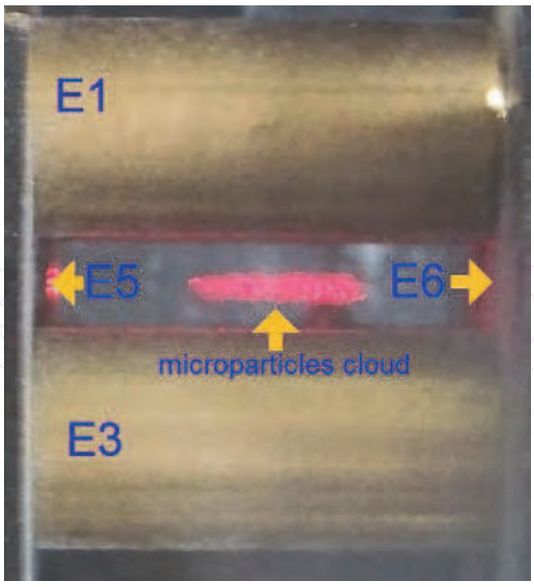

Fig. 2. Microparticles cloud stored along the longitudinal axis of the linear trap

and

$$\frac{d^2y}{d\xi^2} + \delta\frac{dy}{d\xi} + (a_y + 2q_y cos2\xi)y - s_{Ay} = 0 \tag{6}$$

The dimensionless parameters $a_{x,y}$, $q_{x,y}$ and δ are given by:

$$a_x = -a_y = \frac{4QU_0}{M\Omega^2R^2} \tag{7}$$

$$q_x = -q_y = \frac{2QV_0}{M\Omega^2R^2} \tag{8}$$

$$\delta = \frac{6\pi\eta d}{M\Omega} \tag{9}$$

The time dependent functions $s_{Ax}(t)$ and $s_{Ay}(t)$ are given by:

$$s_{Ax}(t) = \frac{4F_{Ax}}{M\Omega^2} \tag{10}$$

$$s_{Ay}(t) = \frac{4F_{Ay}}{M\Omega^2} \tag{11}$$

The pair (a, q) defines the operating point of the electrodynamic trap and determines entirely the characteristics of the particle motion. In the absence of the terms due to the drag force ($-k\frac{dx}{dt}$ and $-k\frac{dy}{dt}$) and the acoustic wave $F_{Ax}(t)$ and $F_{Ay}(t)$, a differential equation of type (5) or (6) is called the *Mathieu equation* (McLachlan, 1947). It can be shown that solutions of a Mathieu equation describe a spatial bounded motion (stable solutions) only for certain regions of the *(a,q)* plane called *stability domains*. This means that, a charged particle can remain indefinitely in the space between the trap electrodes. Additionally, the charged particle trajectory must not cross the electrodes surface implying the supplementary restrictions in its initial position and velocity. One could say that, within the stability domains, a potential

barrier arises preventing the stored charged particles to escape out of the trap. As an example, for the first stability domain, if $a_x = 0$, the stable solutions are obtained if $0 < q_x < 0.908$. The first domain stability corresponds to the lowest voltages applied to the trap electrodes. Due to the air drag area of the first stability domain is enlarged so that, depending on the value of δ, the particle can remain inside the trap even if $q_x > 0.908$. Operation within the higher order stability domains is not practical because of very high voltage to be applied across the trap electrodes. As can be seen in (7) and (8) the operating point depends on the electrodynamic trap geometry, electrodes supply voltages characteristics and charge-to-mass ratio of the stored particle. Knowing the operating point of the trap, its dimensions and applied voltages, then charge-to-mass ratio of the stored particle can be estimated. If $\delta = 0, F_{Ax,y} = 0, |a_x|, |a_y|, |q_x|, |q_y| \ll 1$ (*adiabatic approximation*), the differential equations (5) and (6) have the solutions (Major et al., 2005):

$$x(t) = x_0 cos(\omega_x t + \varphi_x)(1 + \frac{q_x}{2} cos\Omega t) \tag{12}$$

$$y(t) = y_0 cos(\omega_y t + \varphi_y)(1 + \frac{q_y}{2} cos\Omega t) \tag{13}$$

where

$$\omega_x = \frac{\Omega}{2}\sqrt{\frac{q_x^2}{2} + a_x} \tag{14}$$

and

$$\omega_y = \frac{\Omega}{2}\sqrt{\frac{q_y^2}{2} + a_y} \tag{15}$$

Under these conditions the motion of a charged particle confined in a quadrupole trap can be decomposed in a harmonic oscillation at frequencies $\omega_i/2\pi$ called "*secular motion*" and a harmonic oscillation at the frequency $f_0 = \Omega/2\pi$ of ac voltage called "*micromotion*" . As a consequence the motional spectrum of the stored particle contains components $\omega_i/2\pi$ and $f_0 \pm \omega_i/2\pi (i = x, y)$. For arbitrary values of the parameters $a_{x,y}$, $q_{x,y}$ and δ, equations (5) or (6) can be numerically solved.

3. Experimental setup

The experimental setup is based on the method described in (Schlemmer et al., 2001) used for a linear trap. The scheme of the experiment is shown in Fig.3. The output beam of a low power laser module (650 nm, 5 mW) is directed along the longitudinal axis (Oz axis) of the linear trap. A hole drilled through one of the end-cap electrode (E6) allows the laser beam illuminating the axial region of the trap where the stored particles density is maximal and the electric potential is well approximated by the relation (1). A photodetector PD placed outside of the trap and oriented normal to the laser beam receives a fraction of the radiation scattered by the stored particles and converts it into an electrical voltage U_{ph} proportional to the incident radiation intensity. To prevent electrical perturbations due to the existing ac high voltage applied to the electrodes trap, the photodetector is encapsulated in a cylindrical shielding box. The effect of the background light is removed by means of an appropriate electronic circuit. The acoustic excitation of the stored microparticles is achieved by a loudspeaker placed next to the trap. The loudspeaker generates a monochromatic acoustic wave with frequency f_A. In this way both electrical field created by the trap electrodes and the force due to the acoustic wave act simultaneously on the stored microparticles. The motion of the stored particles

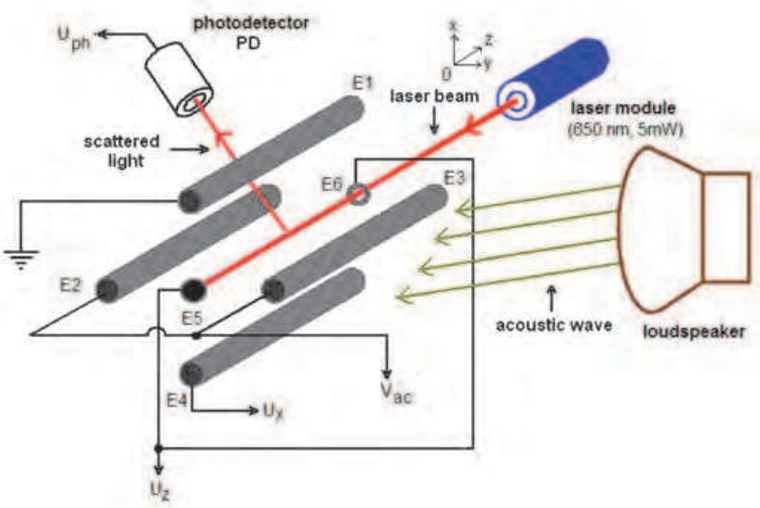

Fig. 3. Schematic of the experimental setup

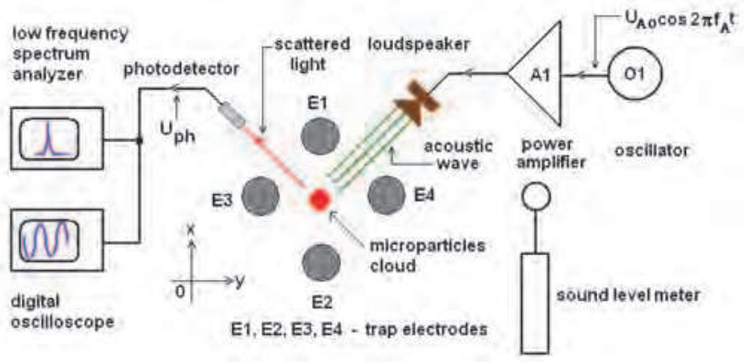

Fig. 4. Block diagram of the measurement chain. The trap electrodes wiring is not shown.

modulates the intensity of the scattered radiation. Therefore the photodetector output voltage U_{ph} contains the same harmonic components. By analysing changes in the structure of the frequency domain spectrum of the voltage U_{ph}, the effect of the acoustic wave on the stored particles can be evaluated. For this purpose a measurement chain whose block diagram is shown in Fig. 4 has been implemented. A digital low frequency spectrum analyser is used to determine the harmonic components of the voltage U_{ph}. The loudspeaker is supplied by the low frequency power amplifier A1 which is driven by the low frequency oscillator O1. The intensity of the acoustic wave is monitored by means of a sound level meter. Both frequency and intensity of the acoustic wave can be varied. A similar version of the experimental setup has been previously described in (Stoican et al., 2008) where preliminary investigations regarding the effect of the acoustic waves on the properties of the microparticles stored in a linear electrodynamic trap particle has been reported.

4. Experimental measurements

The microparticles consist of Al_2O_3 powder, 60-200 μm in diameter, stored at normal pressure and temperature. The working parameters (U_x, U_z and V_0) of the linear trap were chosen so that the magnitude of the harmonic component of the photodetector output voltage U_{ph}

corresponding to f_0 to reach a maximum (Fig. 5a). This operating point of the trap is known as *"spring point"* (Davis et al., 1990). Two typical spectra of the voltage U_{ph} recorded in these experimental conditions are shown in Fig. 6. Only frequencies less than, or equal to $3f_0/2$,

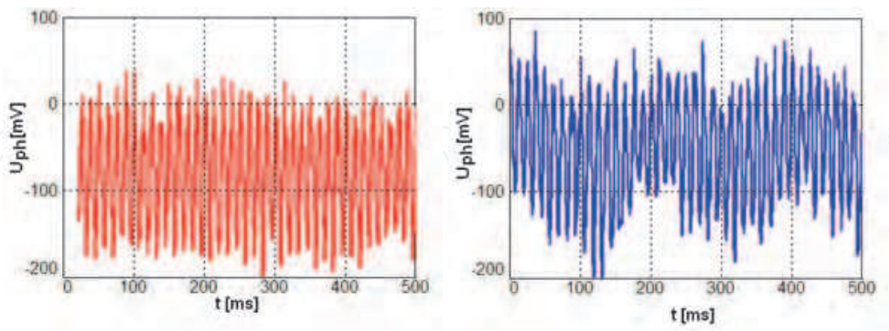

(a) No acoustic excitation

(b) Acoustic excitation, f_A=75Hz. The voltage U_{ph} appears to be amplitude modulated.

Fig. 5. Oscilloscope image representing the time variation of the photodetector voltage output U_{ph} in the absence (a) and presence (b) of the acoustic excitation. Experimental conditions: V_0=3.3kV, U_x=0, U_z=920V, f_0=80Hz. Experimental results.

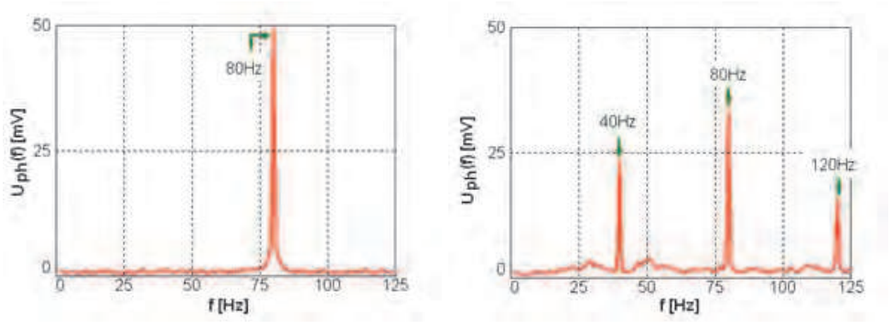

(a) U_z=920V

(b) U_z=100V

Fig. 6. Typical spectra of the photodetector output voltage U_{ph} without the acoustic excitation. Experimental conditions: f_0=80Hz, V_0=3.3kV, U_x=0V. Experimental results.

have been considered because upper lines could be caused by the ac voltage V_{ac} waveform imperfections or digital data processing. Also it was necessary to limit the frequency band to keep a satisfactory resolution of the recordings. As it can be seen from Fig. 6, under these conditions, without the acoustic excitation, the spectra of the photodetector output voltage contain only three significant lines, namely $f_0/2$, f_0 and $3f_0/2$ (here 40Hz, 80Hz and 120Hz). Depending on the applied dc voltages and photodetector position some lines could missing. Several spectra of the photodetector output voltage U_{ph} recorded during acoustic excitation of the microparticles at different frequencies f_A are shown in Fig. 7. The measured sound level was about 85dB. By examining the experimental records, it can be seen that the supplementary lines occur in the motional spectrum of the stored particles. As an empirical rule, the frequency peaks due to the acoustic excitation belong to the combinations of the form $f_0 \pm |f_0 - f_A|$ and $n|f_0 - f_A|$ where n=0, 1, 2..., f_A is the frequency of the acoustic field and f_0 is

the frequency of the applied ac voltage V_{ac}. The rule is valid both for $f_A < f_0$ and $f_A > f_0$. As seen in Fig. 7a and Fig. 7d, the two spectra are almost identical because $|f_0 - f_A|$=20Hz in both cases. If f_A is close to the f_0 the lowest frequency component $|f_0 - f_A|$ yields an amplitude modulation of the voltage U_{ph} very clearly defined (Fig. 5b). The effect is similar to the beat signal due to the interference of two harmonic signals of slightly different frequencies.

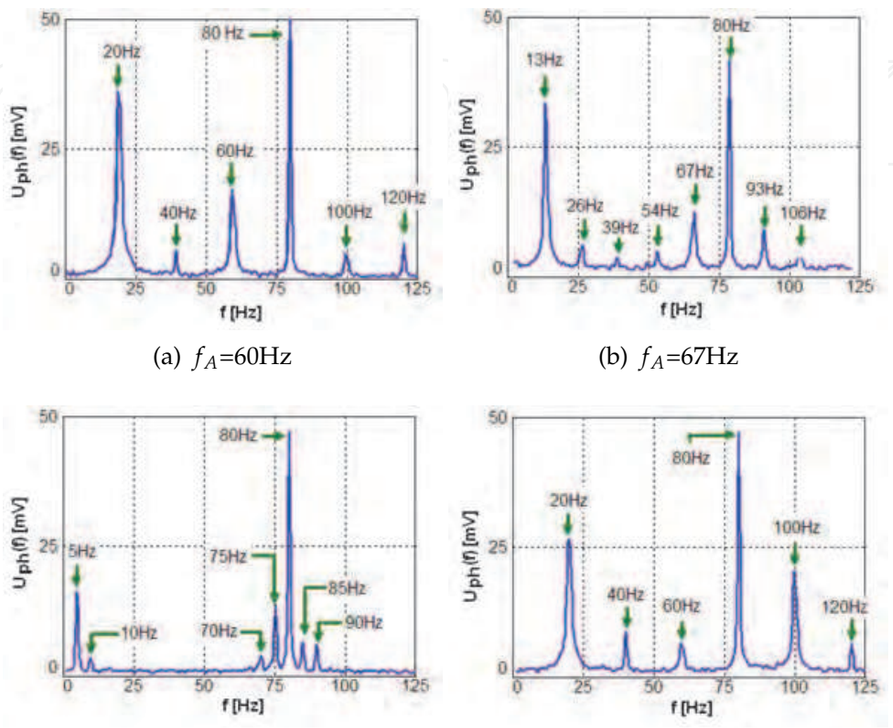

(a) f_A=60Hz (b) f_A=67Hz

(c) f_A=75Hz (d) f_A=100Hz

Fig. 7. Spectrum of the photodetector output voltage U_{ph} when the stored microparticles are excited by an acoustic wave at different frequencies f_A. Experimental conditions: f_0=80Hz, V_0=3.3kV, U_x=0V, U_z=920V, sound level ≈ 85dB. Experimental results.

5. Numerical analysis of the stored particle motion in an acoustic field

A qualitative interpretation of the experimental results requires a numerical analysis on the motion of the stored particles. For this purpose the differential equations (5) and (6) must be numerically solved. Consequently, it is necessary to express functions $s_{Ax}(t)$ and $s_{Ay}(t)$ from (10) and (11) in terms of quantities which are known or can be experimentally measured. A body subjected to an acoustic wave field, experiences a steady force called *acoustic radiation pressure* and a time varying force caused by the periodic variation of the pressure in the surrounding fluid. The radiation pressure is always repulsive meaning that it is directed as the wave vector. The time varying force oscillates at the frequency of the acoustic wave and its time average is equal to zero. The radiation pressure $\overline{F}_R$ exerted on a rigid spherical particle by a plane progressive wave is derived in (King, 1934) as:

$$\overline{F_R} = \frac{\pi^5 d^6}{\lambda^4} \overline{w} F(\rho_0/\rho_1) \tag{16}$$

where d is the particle diameter, λ is the wavelength of the acoustic wave and $\overline{w}$ represents the acoustic energy density. The parameter $F(\rho_0/\rho_1)$ is called *relative density factor* being given by:

$$F(\rho_0/\rho_1) = \frac{1+\frac{2}{9}(1-\rho_0/\rho_1)^2}{(2+\rho_0/\rho_1)^2} \tag{17}$$

where ρ_0 and ρ_1 are air and particle density, respectively. If $\rho_0/\rho_1 \ll 1$, as in the present case (see bellow), practically $F(\rho_0/\rho_1)$=0.305. For a plane progressive acoustic wave, energy density is (Beranek, 1993; Kinsler et al., 2000):

$$\overline{w} = p_s^2/\rho_0 c^2 \tag{18}$$

where p_s is *sound pressure* and c is the speed of propagation of the acoustic wave. Sound pressure can be estimated according to the formula which defines the *sound pressure level* SPL:

$$SPL = 20log_{10}\frac{p_s}{p_{ref}} \tag{19}$$

where p_{ref}=2 x 10^{-5}N/m^2 is the standard reference pressure. Sound pressure level (SPL) is expressed in dB and can be experimentally measured by using sound level meters. In (King, 1934), as an intermediate result, the velocity of a spherical particle placed in an acoustic wave field is given as:

$$\frac{dr}{dt} = -\frac{A_1}{\alpha^3}k_0\frac{\rho_0}{\rho_1}\frac{1}{F_1 - iG_1} \tag{20}$$

where $k_0 = \omega/c$, $\alpha = k_0 d/2$, while $\omega = 2\pi f_A$ is the angular frequency of the acoustic wave. If $\rho_0/\rho_1 \ll 1$ and $\alpha \ll 1$ then $F_1(\alpha) \simeq 2/\alpha^3$ and $G_1(\alpha) \simeq -1/3$. The quantity A_1 is a measure of wave intensity. Assuming a monochromatic plane progressive acoustic wave, the amplitude of the acoustic oscillating force exerted on the particle may be written:

$$F_{A0r} = |M\frac{d^2r}{dt^2}| = \frac{\omega M|A_1|}{\alpha^3}k_0\frac{\rho_0}{\rho_1}\frac{1}{|F_1 - iG_1|} \tag{21}$$

where $|A_1| = 3cv/\omega$. Taking into account expressions for F_1, G_1, $|A_1|$, α and k_0, written above, the relation (21) becomes:

$$F_{A0r} = 2\omega M v\frac{\rho_0}{\rho_1} \tag{22}$$

The quantity v represents the amplitude of the velocity of the surrounding fluid particles (air in this case), which are oscillating due to the acoustic wave, and is related to the sound pressure by the relation:

$$v = \frac{\sqrt{2}p_s}{\rho_0 c} \tag{23}$$

Finally, the amplitude of the oscillating force, considering $\rho_0/\rho_1 \ll 1$ and $\alpha \ll 1$, is:

$$F_{A0r} = \frac{2\sqrt{2}\omega M p_s}{\rho_1 c} \tag{24}$$

Consequently:

$$F_{Ar} = \overline{F_R} + F_{A0r}cos(2\pi f_A t + \beta) \tag{25}$$

As further numerical evaluations will demonstrate the acoustic radiation pressure $\overline{F_R}$ is several order of magnitude less than that of oscillating force amplitude F_{A0r} and has been neglected. In order to simplify theoretical analysis, the weight of the microparticles (i. e. Mg where g=9.8m/s^2) has been also neglected. Experimentally, the microparticles weight are usually compensated by the electric field due to the dc voltage U_x. As a result, considering the experiment geometry (Fig. 4):

$$F_{Ax}(t) = F_{Ay}(t) \approx \frac{\sqrt{2}}{2} F_{A0r} cos(2\pi f_A t + \beta) \tag{26}$$

Therefore the two function $s_{Ax}(t)$ and $s_{Ay}(t)$ takes form:

$$s_{Ax}(t) = s_{Ay}(t) = s_{A0} cos(2\pi f_A t + \beta) = s_{A0} cos(2\frac{f_A}{f_0}\xi + \beta) \tag{27}$$

where

$$s_{A0} = \frac{8\omega p_s}{\rho_1 c \Omega^2} \tag{28}$$

All quantities existing in formula (28) are known or can be experimentally measured. The operating conditions considered for numerical analysis are summarized in Table 2 . The diameter of the Al_2O_3 microparticles can vary in the range from 60μm to 200μm, as

Parameter	Notation	Value
trap inner radius	R	5 x 10^{-3} m
particle density (Al_2O_3)	ρ_1	3700 kg/m^3
air density	ρ_0	1.2 kg/m^3
speed of sound	c	343 m/s
air viscosity	η	1.8 x 10^{-5} kgm^{-1}s^{-1}
sound pressure level	SPL	85 dB
sound pressure	p_s	0.35 N/m^2
sound frequency	f_A	100 Hz
ac voltage frequency	f_0	80 Hz

Table 2. Operating conditions considered for numerical analysis

before mentioned. The two corresponding limit values of the parameters depending on the microparticles size, are shown in Table 3. The operating conditions taken into account are the same as in Table 2. According to numerical values listed in Table 2 and Table 3, $\rho_0/\rho 1 \ll 1$ and

particle diameter d	6 x 10^{-5} m	2 x 10^{-4} m
particle mass M	4.18 x 10^{-10} kg	1.55 x 10^{-8} kg
particle weight Mg	4.10 x 10^{-9} N	1.51 x 10^{-7} N
$\alpha = k_0 d/2$	5.49 x 10^{-5}	1.83 x 10^{-4}
δ	0.09	0.008
acoustic radiation pressure $\overline{F}_R$	2.82 x 10^{-32} N	3.87 x 10^{-29} N
oscillating force amplitude F_{A0r}	2.08 x 10^{-13} N	7.71 x 10^{-12} N
s_{A0}/R	1.11 x 10^{-6}	1.11 x 10^{-6}

Table 3. The limit values corresponding to the particle possible diameter. Operating conditions are listed in Table 2

$\alpha \ll 1$, which are in good agreement with our previous assumptions. Fourier transforms $X(f)$ and $R(f)$, of the rectangular $x(t)$ and radial $r(t) = \sqrt{x^2(t) + y^2(t)}$ coordinates, respectively, in the range from 0 to 125Hz, without the acoustic excitation, obtained by solving numerically differential equations (5) or (6), for several values of the parameters q_x, are shown in Fig.8. Fourier transforms of $x(t)$ and $y(t)$ are similar. As theory of Mathieu equations ascertains, numerical calculations shows that for $|q_{x,y}| \ll 1$, the motional spectrum contains mainly harmonic components due to the secular motion, namely $\omega_x/2\pi$ and $f_0 \pm \omega_x/2\pi$. In practice, the microparticles trapping in such conditions is difficult to be achieved because the potential barrier is too low so that weak external perturbations can eject stored particles out of the trap. The numerical results show that, close to the limit of the first stability domain, the micromotion becomes important and the motional spectrum contains only a few significant lines, namely at f_0 for $r(t)$ and at $f_0/2$ and $3f_0/2$ for $x(t)$, respectively. Fourier transforms $X(f)$ and $R(f)$, of the rectangular $x(t)$ and radial $r(t)$ coordinates, respectively, in the range from 0 to 125Hz, in the presence of the acoustic excitation, obtained by solving numerically differential equations (5) or (6), for several values of the acoustic wave frequency f_A, are shown in Fig. 9. Simulation conditions are listed in Table 4. Expression of the parameter s_{A0}/R corresponds to SLP=85dB and R=5mm. All the remaining parameters, except acoustic wave frequency f_A, are listed in Table 2 and Table 3 The variation of the normalized time

$f_0[Hz]$	q_x	a_x	δ	s_{A0}/R	$r(0)$	$\dot{r}(0)$	β	time interval[s]
80	0.908	0	0.01	0.11 x $10^{-7} f_A[Hz]$	0	0	0	0-40

Table 4. Conditions taken into account to simulate the motion of the a microparticle in the presence of an acoustic field (Figs.9 and 10)

average, $\bar{r}(t)/R$, of the coordinate r as a function of acoustic wave frequency f_A is shown in Fig 10. As on can see from this figure there are two critical frequencies of the acoustic wave, namely $f_0/2$ and $3f_0/2$, where the amplitude of the particle motion rises sharply. It is interesting to note that this very high growth of the motion amplitude does not occur for f_A=f_0. The microparticles cloud appears to form a *non-linear oscillating system* for which resonance frequencies occur at pf_0/q with p and q integer (Landau & Lifshitz, 1976).
The variation of the normalized time average, $\bar{r}(t)/R$, of the coordinate r as a function of $log_{10}(s_{A0}/R)$ at acoustic wave frequency f_A=120Hz is shown in Fig 11. According to (28) and (19) the parameter s_{A0} may be considered a measure of the acoustic excitation because $log_{10}(s_{A0}) = log_{10}p_s + constant$ and sound pressure level SPL depends on $log_{10}p_s$. As on can see from this figure, beyond a threshold value, the average distance from the trap axis grows monotonically with the level of the sound pressure level. Around $s_{A0}/R \simeq 10^{-8}$ there is a threshold value where amplitude of the microparticle motion increases suddenly (the region within the green frame from Fig.11). The transition is not uniform, there are maximum and minimum values of $\bar{r}(t)$. This phenomenon could be interpreted as so called *collapse of resonance* which means that the amplitude of resonance goes to zero for some value of the perturbation amplitude (Olvera, 2001). However numerical result must be regarded with caution. Some hypothesis aimed to simplify mathematical treatment has been introduced. For example it was assumed that the parameter β is equal to zero and it remains constant. In fact β, which signifies the phase shift between ac voltage V_{ac} and acoustic wave, varies randomly because the two oscillations are produced by different generators. Further experiments are necessary to confirm theoretical assertions. All of the numerical results have been obtained by using SCILAB 5.3.1.

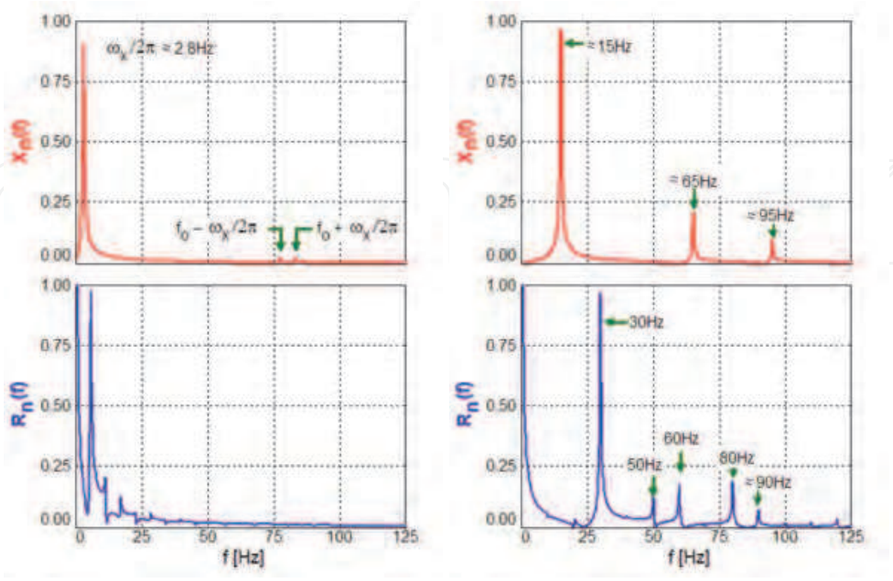

(a) q_x=0.1 (b) q_x=0.5

(c) q_x=0.9 (d) q_x=0.908

Fig. 8. $X_n(f) = X(f)/X_{max}(f)$ (red) and $R_n(f) = R(f)/R_{max}(f)$ (blue) where $X(f)$ and $R(f)$ are Fourier transform of the rectangular $x(t)$ and radial $r(t)$ coordinates, respectively, for $0<f<125$Hz, a_x=0, $f_0 = \Omega/2\pi$=80Hz, δ=0.01, without the acoustic excitation. Numerical result.

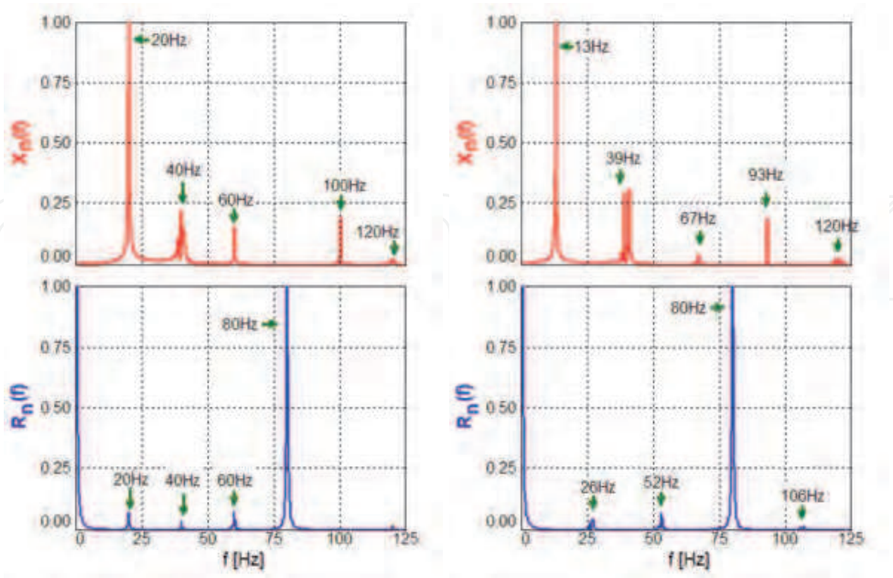

(a) f_A=60Hz

(b) f_A=67Hz

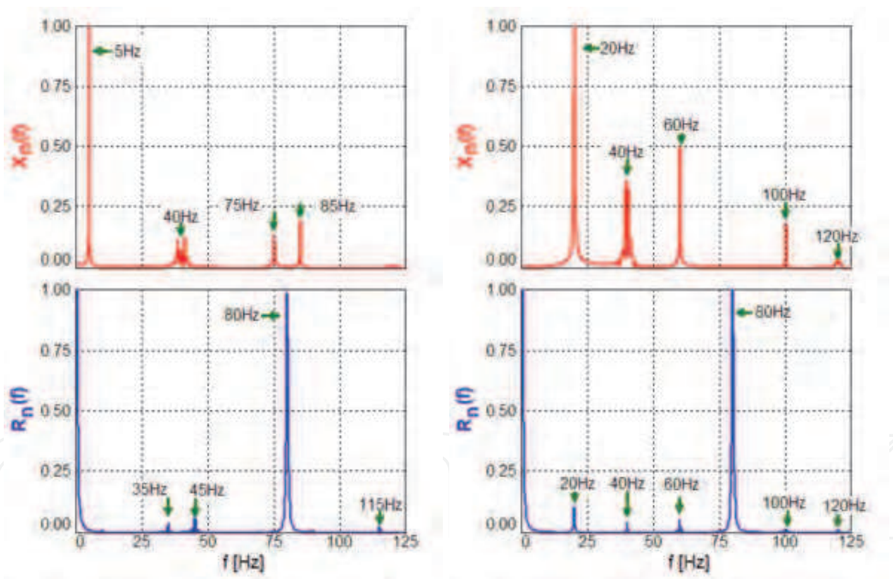

(c) f_A=75Hz

(d) f_A=100Hz

Fig. 9. $X_n(f) = X(f)/X_{max}(f)$ (red) and $R_n(f) = R(f)/R_{max}(f)$ (blue) where $X(f)$ and $R(f)$ are Fourier transform of the rectangular $x(t)$ and radial $r(t)$ coordinates, respectively, for $0<f<125$Hz, in the presence of the acoustic excitation, for several values of the acoustic wave frequency f_A. The plots correspond to the frequency f_0=80Hz of the ac supply voltage V_{ac} and to an incident sound level of 85dB. A complete list of the simulation conditions is displayed in Table 4. Numerical result.

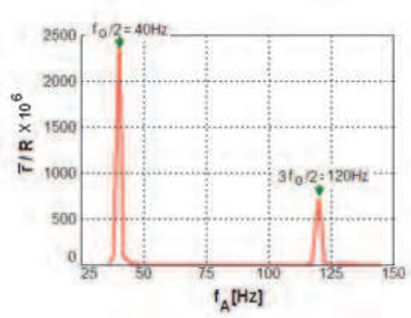

Fig. 10. The normalized time average of the coordinate $r(t)$ as a function of acoustic wave frequency f_A. R represents the inner radius of the linear trap. Simulation conditions are displayed in Table 4. Numerical result.

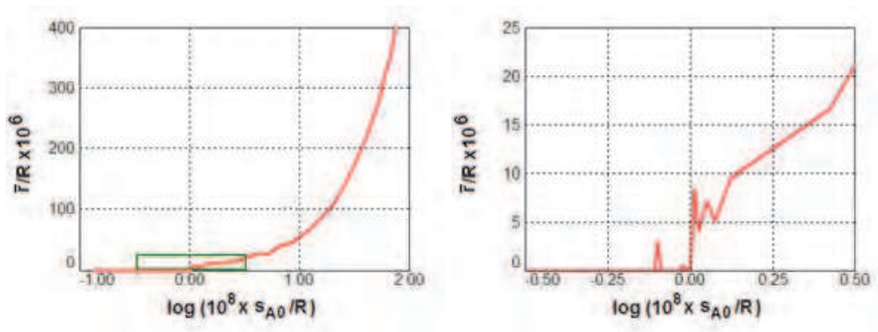

(a) Complete view (b) Expanded view of the region within the green frame

Fig. 11. The normalized time average of the coordinate $r(t)$ as a function of parameter s_{A0}/R at acoustic wave frequency f_A=120Hz. Parameter s_{A0} is a measure of acoustic excitation($log_{10}(s_{A0}) \sim SPL$). Simulation conditions, except parameter s_{A0}/R, are displayed in Table 4. Numerical result.

6. Conclusion

Although measurements result has been interpreted using an approximative and simplified theory of the linear trap, by comparing the experimental spectra with numerical simulations a good qualitative agreement can be noticed. The spectrum of the laser radiation intensity scattered by the stored microparticles seems to be a superposition of the $r(t)$ and $x(t)$ (or $y(t)$) harmonic components, respectively. Because the experimental spectrum obtained without the acoustic excitation, shown in Fig.6 is similar to that displayed in Fig.8d we may suppose that operating point of the linear trap during the experiment corresponds to $q_x \approx 0.908$ (*i.e.* Q/M ≈5.4 x 10^{-4} C/kg cf. (8)). The simulation of the stored particle motion in an acoustic wave has been done taking into account this assumption. By knowing the ratio Q/M and the mass of a microparticle (from Table 3) electric charge Q can be evaluated. Because the microparticles are stored in air at normal pressure, a supplementary restriction on the physical characteristics of the microparticles arises. Assuming that microparticles are spherical and the

electric charge is uniform distributed over its surface, the electric field E_d at the surface is:

$$E_d = \frac{Q}{4\pi\epsilon_0(d/2)^2} \tag{29}$$

where ϵ_0=8.854 x 10^{-12} F/m. Electric charge Q results from:

$$Q = M(\frac{Q}{M}) = \frac{4\pi}{3}(\frac{d}{2})^3\rho_1(\frac{Q}{M}) \tag{30}$$

where Q/M is known. The electric field E_d can not exceed a certain threshold value E_{max}, called *dielectric strength*, at which surrounding gas molecules become ionized, so that the condition $E_d < E_{max}$ is necessary. From (29) and (30), the above condition can be written:

$$d < \frac{6\epsilon_0 E_{max}}{(Q/M)\rho_1} \tag{31}$$

The dielectric strength E_{max} varies with the shape and size of the charged body, humidity and pressure of the air. We consider here the dielectric strength of air E_{max} $\approx$3 x 10^6 V/m. By replacing numerical values in (31), it results that d<69μm. Therefore the diameter of the microparticles which produce the laser beam scattering sensed by the photodetector lies in the range 60-69μm. Distribution of the frequency peaks are almost identical both in experimental recordings and numerical simulation, but their relative heights are different. Besides a simplified theoretical approach, there are a few possible experimental issues. The dc voltages U_x and U_z shift the stored microparticles cloud position relative to the trap axis and, implicitly, to the photodetector aperture. Thus, viewing angle of the photodetector is modified and some harmonic components could not be observed or appear to be very weak. On the other hand, non-uniformity of the frequency characteristic for the common loudspeakers, especially at frequencies below 100Hz, could distort experimental recordings. Numerical estimations demonstrate that, in the described experimental conditions and within the considered range of the acoustic wave frequency, the acoustic radiation pressure $\overline{F}_R$ is very weak compared to the microparticles weight Mg or amplitude of the oscillating force exerted by acoustic wave F_{A0r}(see Table 3). Certainly, the first improvement of theoretical approach would be to add a constant term corresponding to the microparticles weights in differential equations (2) and/or (3), depending on the orientation of the reference system. Like weight, acoustic radiation pressure does not vary in time and can be regarded, mathematically speaking, as a small correction of the microparticles weight. As a result the acoustic radiation pressure is not important here, where only acoustic waves with frequency around frequency f_0 of the ac voltage have been investigated. The acoustic radiation pressure can become significantly at higher frequencies, (see (16)) varying according to f^4. On the other hand, according to the numerical results, if the intensity of the acoustic wave is larger than a threshold value and its frequency has proper values, the amplitude of the stored microparticles motion increases significantly. These frequencies are identical to certain frequency peaks existing in the motional spectrum of the stored particle predicted by the numerical simulations (Fig. 8d) and observed experimentally (Fig.6b). Therefore its action is effective only for the microparticles species whose properties meet certain conditions. In this way, theoretically, the selective manipulation of the stored microparticles by means of the acoustic waves becomes possible.

We gratefully acknowledge material support provided by *Mira Technologies Group SRL - Bucharest, Romania*.

7. References

Beranek, L. L. (1993). *Acoustics*, Acoustical Society of America, New York.

Carleton, K. L., Sonnenfroh, D. M., Rawlins, W. T., Wyslouzil, B. E. & Arnold, S. (1997). Freezing behavior of single sulfuric acid aerosols suspended in a quadrupole trap, *Journal of Geophysical Research* Vol. 102(No. D5): 6025–6033.

Davis, E. J. (1997). A history of single aerosol particle levitation, *Aerosol Science and Technology* Vol. 26(No. 3): 212–254.

Davis, E. J., Buehler, M. F. & Ward, L. T. (1990). The double-ring electrodynamic balance for microparticle characterization,*Review of Scientific Instrument* Vol.61(No. 4): 1281–1288.

Gheorghe, V. N., Giurgiu, L., Stoican, O., Cacicovschi, D., Molnar, R. & Mihalcea, B. (1998). Ordered structures in a variable length a.c. trap., *Acta Physica Polonica A* Vol.93(No. 4): 625– 629.

Jakubczyk, D., Zientara, M., Bazhan, W., Kolwas, M. & Kolwas, K. (2001). A device for light scatterometry on single levitated droplets, *Opto-Electronics Review* Vol. 9(No.4): 423–430.

King, V. L. (1934). On the acoustic radiation pressure on spheres, *Proceedings of the Royal Society (London)* Vol.A147: 212–240.

Kinsler, L. E., Frey, A. R., Coppens, A. B. & Sanders, J. V. (2000). *Fundamentals of Acoustics*, John Wiley and Sons, Inc, New York.

Landau, L. D. & Lifshitz, E. M. (1976). *Mechanics*, Butterworth-Heinemann, Oxford.

Major, F. G., Gheorghe, V. N. & Werth, G. (2005). *Charged Particle Traps, Physics and Techniques of Charged Particle Confinement*, Springer, Berlin Heidelberg New York.

March, R. E. (1997). An introduction to quadrupole ion trap mass spectrometry, *Journal of Mass Spectrometry* Vol. 32: 351–369.

McLachlan, N. W. (1947). *Theory and Application of Mathieu Functions*, Clarendon Press, Oxford.

Olvera, A. (2001). Estimation of the amplitude of resonance in the general standard map, *Experimental Mathematics* Vol.10(No. 3): 401–418.

Pedregosa, J., Champenois, C., Houssin, M. & Knoop, M. (2010). Anharmonic contributions in real rf linear quadrupole traps, *International Journal of Mass Spectrometry* Vol. 290(No. 2-3): 100–105.

Peng, W. P., Yang, Y. C., Kang, M. W., Lee, Y. T. & Chang, H. C. (2004). Measuring masses of single bacterial whole cells with a quadrupole ion trap, *Journal of the American Chemical Society* Vol. 126(No.38): 11766–11767.

Schlemmer, S., Illemann, J., Wellert, S. & Gerlich, D. (2001). Nondestructive high-resolution and absolute mass determination of single charged particles in a three-dimensional quadrupole trap, *Journal of Applied Physics* Vol. 90(No. 10): 5410–5418.

Shaw, R. A., Lamb, D. & Moyle, A. M. (2000). An electrodynamic levitation system for studying individual cloud particles under upper-tropospheric conditions, *Journal of Atmospheric and Oceanic Technology* Vol. 17(No. 7): 940–948.

Stoican, O. S., Dinca, L. C., Visan, G. & Radan, S. (2008). Acoustic detection of the parametrical resonance effect for a one-component microplasma consisting of the charged microparticles stored in the electrodynamic traps, *Journal of Optoelectronics and Advanced Materials* Vol.10(No. 8): 1988–1990.

Stoican, O. S., Mihalcea, B. & Gheorghe, V. N. (2001). Miniaturized microparticle trapping setup with variable frequency, *Roumanian Reports in Physics* Vol. 53(No. 3-8): 275–280.

Wuerker, R. F., Shelton, H. & Langmuir, R. V. (1959). Electrodynamic containement of charged particles, *Journal of Applied Physics* Vol. 30(No. 3): 342–349.

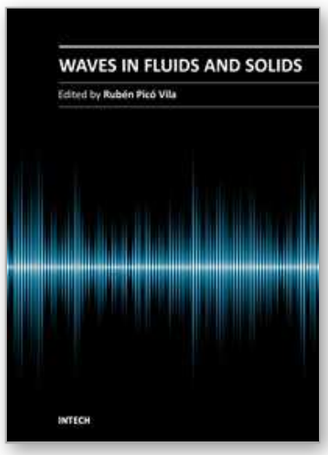

Waves in Fluids and Solids
Edited by Prof. Ruben Pico Vila

ISBN 978-953-307-285-2
Hard cover, 314 pages
Publisher InTech
Published online 22, September, 2011
Published in print edition September, 2011

Acoustics is an discipline that deals with many types of fields wave phenomena. Originally the field of Acoustics was consecrated to the sound, that is, the study of small pressure waves in air detected by the human ear. The scope of this field of physics has been extended to higher and lower frequencies and to higher intensity levels. Moreover, structural vibrations are also included in acoustics as a wave phenomena produced by elastic waves. This book is focused on acoustic waves in fluid media and elastic perturbations in heterogeneous media. Many different systems are analyzed in this book like layered media, solitons, piezoelectric substrates, crystalline systems, granular materials, interface waves, phononic crystals, acoustic levitation and soft media. Numerical methods are also presented as a fourth-order Runge-Kutta method and an inverse scattering method.

InTech Europe
University Campus STeP Ri
Slavka Krautzeka 83/A
51000 Rijeka, Croatia
Phone: +385 (51) 770 447
Fax: +385 (51) 686 166
www.intechopen.com

InTech China
Unit 405, Office Block, Hotel Equatorial Shanghai
No.65, Yan An Road (West), Shanghai, 200040, China
中国上海市延安西路65号上海国际贵都大饭店办公楼405单元
Phone: +86-21-62489820
Fax: +86-21-62489821

IntechOpen